

SCINTILLATION BASED SEARCH FOR OFF-PULSE RADIO EMISSION FROM PULSARS

KUMAR RAVI ¹, AVINASH A. DESHPANDE¹

¹Raman Research Institute, Bangalore, India; raviranjan@rri.res.in; desh@rri.res.in

Draft version September 26, 2021

ABSTRACT

We propose a new method to detect off-pulse (unpulsed and/or continuous) emission from pulsars, using the intensity modulations associated with interstellar scintillation. Our technique involves obtaining the dynamic spectra, separately for on-pulse window and off-pulse region, with time and frequency resolutions to properly sample the intensity variations due to diffractive scintillation, and then estimating their mutual correlation as a measure of off-pulse emission, if any. We describe and illustrate the essential details of this technique with the help of simulations, as well as real data. We also discuss advantages of this method over earlier approaches to detect off-pulse emission. In particular, we point out how certain non-idealities inherent to measurement set-ups could potentially affect estimations in earlier approaches, and argue that the present technique is immune to such non-idealities. We verify both of the above situations with relevant simulations. We apply this method to observation of PSR B0329+54 at frequencies 730 and 810 MHz, made with the Green Bank Telescope and present upper limits for the off-pulse intensity at the two frequencies. We expect this technique to pave way for extensive investigations of off-pulse emission with the help of even existing dynamic spectral data on pulsars and of course with more sensitive long-duration data from new observations.

Subject headings: scattering — methods: observational — pulsars: general — pulsars: individual (B0329+54) — radio continuum: general — ISM: general — techniques: high angular resolution

1. INTRODUCTION

It is the pulsed nature of the emission (as against continuous emission) that made the discovery of pulsars (Hewish et al. 1968) possible. Their average intensities, if were to manifest as continuous emission, are in most cases too weak to be detectable, in presence of possible confusion from other continuous sources. The pulsed emission has been studied in great detail, and has lead to our present understanding of the physical picture of pulsars. However, the question as to whether pulsar radiation indeed has any intrinsic continuous component, in addition to its distinguishing pulsed signature, or if the periodic emission extends well beyond the main/inter-pulse windows, have been issues of much interest since the early days of pulsar studies.

There have been several attempts to detect off-pulse emission from pulsars (as summarized in Table 3 and discussed in Section 5 of Basu et al. 2011). Most attempts were primarily aimed at

detection of unpulsed emission component of magnetospheric origin (for example, Huguenin et al. 1971; Bartel et al. 1984; Perry & Lyne 1985; Hankins et al. 1993; Basu et al. 2011,2012), which is indeed the focus of this paper. In contrast, some were prompted by, and were aimed to test, the proposition of Blandford et al. (1973) - “existence of ghost supernova remnants around old pulsars”. Detection of unpulsed emission of magnetospheric origin is indeed challenging, when based on apparent intensity in the off-pulse region, particularly in presence of a variety of unresolved astronomical sources and the resulting *confusion*. Such contaminants could include pulsar companions, if any, nearby galactic/extragalactic radio sources, and diffuse background emission, in addition to the following sources associated with the pulsar. They may include (e.g. as discussed by Hankins et al. 1993) weak halos (Blandford et al. 1973), remnants of the progenitor supernova, shock structures or synchrotron nebulae, and detectable bow

shock. All these contaminations are unavoidable because of finite beam-width of single-dish telescopes and non-negligible side-lobes of interferometers.

After several non-detections and some reports of detections that were refuted subsequently, the off-pulse emission has attracted renewed attention with Basu et al. (2011, 2012) reporting detection of off-pulse emission from B0525+21 and B2045-16 based on their GMRT observations. It is worth noting, that in their study of 20 pulsars, including B0329+54, B0525+21 and B2045-16, at 2.7 and 8.1 GHz using the NRAO 3-element interferometer, Huguenin et al. (1971) found no significant unpulsed emission, implying an upper limit of 20 mJy within 10 arcsec of the pulsar directions. Much later, Bartel et al. (1984) made observations of pulsars B0329+54 and B1133+16 at 2.3 GHz using Mark III VLBI, and also ruled out continuous emission above their detection limit (2.5 mJy). Soon after, Perry & Lyne (1985), reported their interferometric observations at 408 MHz, on 25 pulsar including B0329+54 and B0525+21, made using 76m MK 1A telescope at Jodrell Bank and the 25m telescope at Dafford, with baseline of 127 km. They claimed detection of unpulsed emission from 4 pulsars B1541+09, B1929+10, B1604-00 and B2016+28. However, later it became clear that B1541+09 and B1929+10 are aligned rotators (Hankins et al. 1993; Rathnasree & Rankin 1995), and the unpulsed emission from B1604-00 and B2016+28 were shown to be from unrelated background sources (Strom & Van Someren Greve 1990; Hankins et al. 1993).

The recently reported detections of off-pulse emission (Basu et al. 2011; 2012) from two long period pulsars B0525+21 (3.75 s) and B2045-16 (1.96 s) are based on the imaging mode of GMRT, and also at two frequencies (325 and 610 MHz). Although the authors have discussed some effects that could potentially contaminate off-pulse region with leakage from the emission that is otherwise confined to the main-pulse window, and have attempted some tests based on which they claim absence of such leakage. We consider these tests inadequate to rule out “leakage”, since there are a few different aspects, associated with commonly employed receiver setups, that have noticeable potential for undesirably spilling the main pulse contribution across off-pulse region.

Ideally, we need a method that is immune to such contamination, as far as possible, while mak-

ing reliable estimation of possible off-pulse or unpulsed emission intrinsic to pulsar.

Owing to their compact size and pulsed emission, pulsars have been an excellent probe of the ISM since their discovery. Primarily, they have revealed the distribution of free electron in the Galaxy, through direct measures of column density (from the observed dispersion) and spatial distribution of electron density irregularities (from scintillations and angular/temporal broadening as a result of scattering). The highly polarized nature of their radiation also allows Faraday Rotation measurements, sampling the magneto-ionic component of the intervening medium, and their pulsed nature facilitates some of the clearest measurements of HI absorption along their sight-lines. Of these, the diffractive scintillation effects are readily observable in pulsar directions thanks to their tiny angular sizes, and become apparent only in the cases of some extra-galactic sources having the required compact angular size, such as in early phases of γ -ray burst (GRB) afterglow sources (see for example, Frail et al. 1997; Macquart & de Bruyn 2006).

The diffraction induced chromatic modulation of intensity, when combined with relative motions, translates to intensity variations across time and frequency. Similarly it is only the pulsed nature of the radio pulsars which makes the dispersion effect measurable, and also to reveal the temporal broadening due to scattering. However, the latter can be probed indirectly via other manifestation of scattering (such as decorrelation scales in frequency and/or angular broadening), even in the case of continuous sources. The *camaraderie* between the pulsars and the interstellar medium is indeed reciprocal. For example, ultra-high angular resolution probe of pulsar emission is made possible by the ISM acting as a lens. This was first pointed out by Lovelace (1970) and has been followed-up by many (e.g. Cordes & Wolszczan 1988; Pen et al. 2014; and references therein). Here, the diffractive/refractive effects due to large scale irregularities are considered as providing interstellar interferometric measurements capable of resolving even magnetospheric emission regions of pulsars. The refractive effects leading to multiple imaging manifest themselves as fine-scale corrugations or drift patterns within scintles in the dynamic spectra resulting from diffractive scintillations (e.g. Wolszczan and Cordes 1987, Gupta et al. 1994, 1999).

In this paper, we present a technique which advantageously uses such interstellar-scale telescope for search and detection of unpulsed emission, if any, from pulsars. Our technique (described in Section 2) is based on diffractive interstellar scintillation (DISS) and its correlated imprint on the pulse intensity and any off-pulse emission intrinsic to the pulsar, and has the potential for providing more reliable measurement of intrinsic off-pulse/unpulsed emission, without needing conventional interferometric measurements, i.e. which are possible even with single-dish observations.

In Section 3, we demonstrate sensitivity of our technique using simulated dynamic spectra over wide band, and assess its immunity to various known sources of contamination in the off-pulse region. Discussion of one such potential contaminant is given in Appendix A. The details of the DISS simulation are presented in the Appendix B. In Section 4, we illustrate application of our technique to real data, using observations on B0329+54 at two radio frequencies. We summarize the main conclusions of our paper in Section 5.

2. SCINTILLATION-BASED TECHNIQUE FOR SEARCH/DETECTION OF UNPULSED EMISSION FROM PULSARS

In this section, we present a new technique based on diffractive interstellar scintillation (DISS) and assessment of correlation between dynamic spectra for the pulse and off-pulse intensities. It effectively renders measurements with fine angular resolution offered by interstellar diffraction to distinguish pulsar emission region from sources of confusion, even in close proximity to the pulsar. This DISS correlation criterion effectively and readily discriminates against all discrete and diffuse radio emissions on angular scales larger than that of the pulsar magnetosphere, since they will be devoid of DISS imprint in their dynamic spectra, let alone show any correlation with pulse intensity variations. Any confusing compact source, unresolved by the observing telescopes, and compact enough to show DISS, will show a dynamic spectral signature, i.e., the scintillation pattern, significantly different from that associated with the pulsar emission. In fact, differences between the scintillation patterns associated with even the different components within the pulse profile have been probed to assess spatial separation, if any, between the apparent sites of emission (Cordes et al. 1983).

If indeed, a pulsar has a component of intrinsic emission that is unpulsed/continuous, we expect its intensity modulation due to interstellar scintillation to be closely related to, if not matching, that of the pulsed component. For the desired correlation to exist between the diffractive scintillation spectra of intensities in the two longitude regions, the spatial transverse separation between the associated emission regions should ideally be well within the equivalent spatial resolution of the interstellar aperture/interferometer at work. As Cordes et al. (1983) have already noted, the spatial scale S_d of the diffraction pattern in the observer plane also (reciprocally) defines the associated spatial resolution at the source distance.

A suitable data set for implementation of our technique is, in general, an appropriately sampled data cube of intensity $I(\nu, t, \phi)$, as a function of rotational longitude ϕ , radio frequency ν and time t , and over wide frequency and time spans of, say, $\Delta\nu_{\text{BW}}$ and Δt_{obs} , respectively.

The two dynamic spectra, $\bar{I}_{\text{on}}(\nu, t)$ and $\bar{I}_{\text{off}}(\nu, t)$, to be tested for mutual correlation, are to be constructed for the apparent average intensity across (i) an appropriate number of bins spanning or within the pulse window, and (ii) a chosen set of bins or longitude range in the off-pulse region which is well-separated from the pulse window. All of the (dynamic) spectra here are assumed to be already corrected for any non-uniformity in spectral response of the observing system within the observed band.¹

Sensitivity in the estimation of correlation depends on the signal-to-noise ratio in estimation of the two dynamic spectra, and the degrees of freedom provided by the richness in the dynamic spectra, quantifiable to the first order in terms of number of scintles. Naturally, scintillation dynamic spectra obtained from longer duration observations with wide spectral coverage are desired, if not essential. The dynamic spectral resolutions in time and frequency, say, δt_{res} and $\delta\nu_{\text{res}}$, respectively, need to be adequately finer than the respective decorrelation scales (t_s and ν_d), which together characterize the average *size* of scintles. The dynamic spectra, therefore, are to be

¹ An estimate of the required *normalized* spectral gain response ($G(\nu)$), to be used for dividing all the observed spectra, can be made by averaging the observed off-pulse spectra over the entire time span of observation to first obtain a mean uncalibrated spectrum $\langle S_{\text{off}} \rangle(\nu)$, and then normalizing it with band-averaged intensity \bar{S}_{off} , such that $G(\nu) = \langle S_{\text{off}} \rangle(\nu) / \bar{S}_{\text{off}}$.

smoothed optimally to reduce the uncertainty in estimation of the intensity variations due to scintillation, without washing out details in the ISM induced diffractive variation of interest.

In practice, the dynamic spectra are not free of (additive) random noise in estimating intensity at each pixel in the time-frequency plane, but the magnitude of this noise is expected to be largely consistent with the system temperature and the integration employed (quantified by the relevant time-bandwidth product). Thus, in general, $I_{\text{on}}(\nu, t) = I_{\text{on}}^p(\nu, t) + U_{\text{on}}(\nu, t)$, and $I_{\text{off}}(\nu, t) = I_{\text{off}}^p(\nu, t) + U_{\text{off}}(\nu, t)$, where the U_{on} and U_{off} represent random noise (with zero mean and standard deviations σ_{on} and σ_{off} respectively), which is uncorrelated from pixel to pixel, and contaminates the respective underlying pulsar dynamic spectra I_{on}^p and I_{off}^p . These delta-correlated noise contributions, of magnitude σ_{on}^2 and σ_{off}^2 , will be clearly noticeable as such at zero-lag in the respective auto-correlation functions, ACF_{on} and ACF_{off} , of the dynamic spectra, on top of the the otherwise smoothly varying auto-correlations of I_{on}^p and I_{off}^p , respectively. Hence, the zero-lag auto-correlation of the underlying intensity variation is estimated routinely by interpolation from correlations at adjacent lags.

The average cross-correlation between the intensity variations in two dynamic spectra, $I_{\text{on}}(\nu, t)$ and $I_{\text{off}}(\nu, t)$, defined as

$$CC(0, 0) = \langle \delta I_{\text{on}}(\nu, t) \delta I_{\text{off}}(\nu, t) \rangle \quad (1)$$

at zero lags, is to be assessed for significance against uncertainties, where $\delta I_{yy}(\nu, t) = I_{yy}(\nu, t) - \langle I_{yy} \rangle$ for yy state (*on* or *off*), and $\langle x \rangle$ indicates ensemble average of x across the span of (ν, t) . The uncertainty in the estimated correlation, in the best case (i.e. dynamic spectra free of noise and other undue contaminants), will be dominated finally by the finiteness of available scintle statistics. In case of detection of significant correlation, the off-pulse emission intensity as fraction η of on-pulse intensity can be estimated as

$$\begin{aligned} \eta &= \frac{\langle \delta I_{\text{on}}(\nu, t) \delta I_{\text{off}}(\nu, t) \rangle}{\langle (\delta I_{\text{on}}(\nu, t))^2 \rangle} \\ &= \frac{CC(0, 0)}{AC_{\text{on}}(0, 0) - \sigma_{\text{on}}^2} \end{aligned} \quad (2)$$

where $AC_{\text{on}}(0, 0)$ is the average zero-lag auto-correlation of (on-)pulse intensity variations, which includes the variance σ_{on}^2 of the delta-correlated noise $U_{\text{on}}(\nu, t)$.

In the discussion so far, the apparent intensity fluctuations across the dynamic spectrum for the on-pulse region are, in an ideal case, assumed to be primarily a manifestation of the interstellar scintillations across the observing band. However, a finite but small part of these may be due to 1) variations in the system noise, including the sky noise (other than that from the pulsar), in addition to 2) the contribution from aliased spectral range, if any. The former additive contributions equally affect the dynamic spectrum for the off-pulse region, and may undesirably contribute to the apparent correlation between the dynamic spectra. It is therefore important that the *on-pulse* dynamic spectrum $I_{\text{on}}(\nu, t)$ is obtained after subtraction of $I_{\text{off}}(\nu, t)$ from the corresponding spectrum for the on-pulse region. The version of $I_{\text{off}}(\nu, t)$, to be used for subtraction here, should be for intensity averaged over the entire off-pulse region, as far as possible. In case of any genuine unpulsed intensity with correlated variations with those for on-pulse region, the suggested subtraction would result in an under-estimation of η by an amount η^2 . On the other hand, even intrinsic variations in the off-pulse region that are uncorrelated between the two dynamic spectra would be unduly subtracted from the on-pulse dynamic spectrum, and would introduce a negative bias in η estimate. The magnitude of such bias is given by the ratio of variance σ_U^2 of these uncorrelated variations in the off-pulse spectrum to that for variations in the on-pulse spectrum (i.e. $\sigma_U^2 / (AC_{\text{on}}(0, 0) - \sigma_{\text{on}}^2)$). In any case, the negative bias will be limited to η_{max}^2 , where η_{max} is as defined later in the Equation 6. The advantage of thus removing any common unpulsed intensity variations, either due to sky or system, from $I_{\text{on}}(\nu, t)$, in terms of obtaining a more reliable estimate of η , overwhelms the undesirability of the the mentioned bias, which is expected to be insignificant any way.

Of course, any intrinsic variability in the pulsar intensity would leave an unavoidable (multiplicative) imprint in the dynamic spectrum. The spectral scales of intrinsic variability are expected to be much wider than those associated with interstellar scintillation. There is no a priori basis yet for expecting the possible unpulsed component, if any, to have correlated intrinsic variability. Hence, in general, any independent intrinsic variability of intensities in the two regions would reduce the net cross-correlation, and in any case, increase the uncertainty in the estimation of the unpulsed in-

tensity. Fortunately, any pulse-to-pulse variations in intrinsic intensity are expected to average out, with suitable temporal smoothing of the dynamic spectrum ($P \ll \Delta t_{\text{res}} < t_s$). Any residual variation, on time scales shorter than Δt_{res} , would be indistinguishable from the random uncertainty in estimation of the dynamic spectral elements. The combined magnitude of these fluctuations would be readily apparent in the auto-correlation function across the first few time-lags, as the delta-correlated contribution. In comparison, the auto-correlation due to scintillation-induced intensity variations is expected to decorrelate on a relatively longer time-scales (t_s).

The expected implicit linear inter-relationship between the patterns (after removing the respective mean values), assessed through formal cross-correlation, can be modeled explicitly as follows

$$\delta I_{\text{off}}(\nu, t) = \eta \delta I_{\text{on}}(\nu, t) + U(\nu, t) \quad (3)$$

where, the first term on the right-side is the best-fit model, and $U(\nu, t)$ is the apparent deviation or the part of observed off-pulse dynamic spectrum that is uncorrelated in time and frequency with $\delta I_{\text{on}}(\nu, t)$, with its nominal mean $\langle U(\nu, t) \rangle = 0$, and other quantities as defined earlier. The uncorrelated part $U(\nu, t)$ includes also any measurement uncertainties in I_{off} and also the model ηI_{on} . In the above formulation, as in the Equation 2, η is a measure of the ratio $\delta I_{\text{off}}/\delta I_{\text{on}}$.

The uncertainty σ_η in its estimate can be expressed as

$$\sigma_\eta = \frac{\sigma_{\langle U \rangle}}{\sqrt{\langle (\delta I_{\text{on}}(\nu, t))^2 \rangle}} \quad (4)$$

where $\sigma_{\langle U \rangle}$ is the reduced uncertainty in the mean of $U(\nu, t)$, and is related to standard deviation in $U(\nu, t)$ as

$$\sigma_{\langle U \rangle} = \sigma_U \sqrt{\frac{1}{N_{\text{eff}}}} \quad (5)$$

where N_{eff} is the effective size of the ensemble. The $\langle U \rangle$ and σ_U are, in practice, computed using all of the N samples available in the dynamic spectral array, including $U(\nu, t)$. The total number of points N in these arrays is equal to $N_{\nu 0} N_{t 0}$, where $N_{\nu 0}$ is the number of spectral channels and $N_{t 0}$ number of time bins/sections in the dynamic spectrum. However, since all the points/pixels in the dynamic spectrum are not independent, particularly when the random measurement noise is much smaller than the intensity variations due to scintillation. Hence, in such

cases, N_{eff} is often much smaller than N , and represents rather the number of independent samples in the dynamic spectrum. We have used the number of scintles as defining N_{eff} , so that our uncertainty estimate σ_η corresponds to worst-case error. The definition of number of scintles, as given in Cordes & Lazio (1991), is $N_{\text{eff}} = N_t \times N_\nu$, where $N_t = 1 + \kappa(\Delta t_{\text{obs}}/t_s)$, $N_\nu = 1 + \kappa(\Delta \nu_{\text{BW}}/\nu_d)$, where κ is an empirically obtained number (we can call it *filling factor*), lies in range 0.1 – 0.5. If N_{eff} for one spectrum is different from that for the other, we use the geometric mean of the two N_{eff} values.

For dynamic spectra spanning long durations, explicit attention would be needed to examine if they are affected by possible slow variations in pulse intensity within the span, due to intrinsic variations and/or originating from extrinsic reasons, including refractive scintillations and any instrumental gain variations that remain to be corrected. The correlation scales across frequency for these are expected to be generally wide. Hence, any contamination in the off-pulse region, as mentioned above, is likely to be modulated the same way, resulting in spurious correlation corrupting the correlation of interest. It may become necessary therefore to either estimate slow modulation, and correct at least the on-pulse dynamic spectra accordingly, or estimating the correlation or η using dynamic spectra of shorter spans at a time, repeating the analysis for each of such sections separately, and then computing a weighted average of η , combining independent estimates made using subsets of data.

Before proceeding further, we wish to draw attention to a particular ready utility of the dynamic spectra of the apparent intensity variations in the on-pulse and off-pulse regions. We argue that, regardless of the details of contamination, and the presence or the lack of correlation between the two dynamic spectra, it is possible to define a hard upper-limit for the unpulsed intensity, as

$$\begin{aligned} \eta_{\text{max}} &= \sqrt{\frac{\langle \delta I_{\text{off}}(\nu, t)^2 \rangle}{\langle (\delta I_{\text{on}}(\nu, t))^2 \rangle}} \\ &= \sqrt{\frac{AC_{\text{off}}(0, 0) - \sigma_{\text{off}}^2}{AC_{\text{on}}(0, 0) - \sigma_{\text{on}}^2}} \end{aligned} \quad (6)$$

where $AC_{\text{off}}(0, 0)$ is the average zero-lag auto-correlation of observed intensity variations in the off-pulse region, which includes the variance σ_{off}^2 of the delta-correlated noise $U_{\text{off}}(\nu, t)$.

When $AC_{\text{off}}(0,0) \gg \sigma_{\text{off}}^2$, fractional uncertainty (1σ) in η_{max} would be $1/\sqrt{2N_{\text{eff}}}$. However, even when $\delta I_{\text{off}}(\nu, t)$ appears to consist of only delta-correlated noise, i.e. $\eta_{\text{max}} \approx 0$, the uncertainty would at best be limited to $\sigma_{\text{off}}/\sqrt{N} < (\delta I_{\text{on}}(\nu, t))^2 >$.

2.1. Implications of relative location of possible off-pulse emission region

In general, the apparent emission in the off-pulse region would be a combination of the intrinsic and confusing sources of continuous emission, and the discussed correlation would be correspondingly partial, but providing a measure of the intrinsic component (spatially confined within the transverse scale S_d).

Given the form of spatial distribution of electron density irregularities in the ISM as detailed in Appendix B, this spatial resolution scale S_d , same as the diffraction pattern scale, is given by the following relation (Armstrong et al. 1995).

$$S_d = [8\pi r_e^2 \lambda^2 C_N^2 z f(\alpha)/(\alpha + 1)]^{-1/\alpha} \quad (7)$$

where, r_e is the classical radius of electron, λ is the radio wavelength, $\alpha = \beta - 2$, and z is the effective propagation distance through the ISM.²

The ISM parameters in the above equation are not directly measurable, although can be estimated.³ A related and more readily measurable quantity is the scintillation decorrelation bandwidth ν_d , or alternatively the temporal scatter broadening τ of the pulse, where $\tau = z\theta^2/2c \approx 1/2\pi\nu_d$, and c is the speed of light. Thus, S_d can be estimated from ν_d measurement, as⁴

$$S_d = \sqrt{z\lambda^2\nu_d/4c\pi} = r_f \sqrt{\nu_d/2\nu} \quad (8)$$

where $r_f (= \sqrt{z\lambda/2\pi})$ is the Fresnel scale, and ν is the observing radio frequency.

² For uniformly distributed scattering, z would correspond to the distance to the pulsar. For Kolmogorov turbulence, $\beta = 11/3$ ($\alpha = 5/3$) and the numerical value of the function $f(\alpha)$ is ≈ 1.12 .

³ The diffractive scintillation time-scale t_s (decorrelation time) is directly related to S_d , where $t_s = S_d/V$, but the equivalent velocity V of the medium relative to the pulsar sight-line is not independently known in most cases. On the other hand, the associated angular scatter broadening θ , which ultimately limits the resolution in imaging observations, also relates to the above spatial scale, as $\theta = \lambda/2\pi S_d$.

⁴ The form of this expression is consistent with that in Equation 13 of Cordes et al. (1983).

A positive result in our proposed correlation test would not only conclusively confirm the claimed detections, but would constrain the apparent size and spatial separation, at the so-called “retarded emission time” (Cordes et al. 1983), between the corresponding emission regions, and the level of correlation would provide clues on the relative spatial separation. A negative result, on the contrary, would not necessarily imply absence of unpulsed emission, unless the resolution scale S_d is large enough to cover the entire spatial extent within which emission can be considered as intrinsic to the pulsar. Considering the maximum separation between relevant emission regions to be the so-called light-cylinder radius r_L ($= cP/2\pi$), the above requirement implies that $r_L \lesssim S_d$, where P is the pulsar period⁵.

This condition can also be expressed as $cP/2\pi \lesssim r_f \sqrt{\nu_d/2\nu}$, assessment of which would require an estimate of z , in addition to that of the decorrelation bandwidth ν_d . Although independent distance measurement is desired, z estimated from dispersion measure would also render useful for the present purpose. It is worth emphasizing that the above stated condition is not model dependent, i.e. independent of β .

For a given pulsar, i.e. given P , z and C_N^2 , the observing frequency ν can be chosen suitably, to see if the above condition can be met. The condition is more likely to be satisfied in cases of higher frequency probe of scintillation patterns for relatively nearby short-period pulsars.⁶

In any case, if any intrinsic unpulsed emission were to originate within the angular scale S_d/z around the pulsar, we expect to find the expected correlation signature. Although such cross-correlation (at zero-lag) is expected to fall significantly and rapidly, as $\exp[-(\Delta S/S_d)^{(\beta-2)}]$ (Cordes et al. 1983), with increasing separation ΔS . However, if the separation, even if large (i.e. many times S_d), happens luckily to be near parallel (within angle $(S_d/\Delta S)^c$, for $S_d \leq \Delta S$), then again significant cross-correlation would be

⁵ For the spin periods in the range 1.4 ms–11.8 s, the range of light-cylinder radius corresponds to $\sim 10^4$ – 10^8 m.

⁶ The underlying basic dependencies, as in the Equation 7, imply that the spatial resolution scale S_d broadens with increasing radio frequency (ν) and with decreasing integrated scattering measure $C_N^2 z$. This diffraction pattern scale, in the weak scattering regime at adequately high frequencies, would of course saturate to its upper limit, that is the Fresnel scale r_f , equal then to the refractive scale at its lower limit.

expected, but now at time-lag $\Delta t \sim t_s \Delta S / S_d$, if the scattering *transfer function* can be considered as essentially *frozen* over those time scales. The above considerations necessitate exploration of the discussed correlation over a range of lags in both time and frequency, as we do in our tests and analysis to follow.

3. TESTS WITH SIMULATED DYNAMIC SPECTRA: ASSESSMENT OF SENSITIVITY AND IMMUNITY

Here, we illustrate application of our technique to simulated scintillation dynamic spectra, and assess its performance, in terms of ability to reliably estimate off-pulse/unpulsed intensity intrinsic to the pulsar, and immunity to potential contaminants in the off-pulse region.

As mentioned in Section 2, and illustrated in Appendix A, one of the subtle contamination of the off-pulse region could come from genuine main-pulse signal itself, if it is not adequately filtered out from the spectral regions beyond the observing band. These aliased contributions (from possible image bands relevant to heterodyning, and regions inadequately attenuated by band-defining filter before digitization) appear at longitudes that are, in general, offset from the main-pulse window (see Figure A1), depending on dispersion measure and frequency separation.

Fortunately, the scintillation-induced intensity pattern would significantly differ for spectral separations larger than the decorrelation scales, ν_d , particularly when $\nu_d \ll \Delta\nu_{BW}$, and even the overall shape and sizes of the scintles (characterized by the decorrelation scales, ν_d and t_s), themselves vary systematically with ν , more rapidly with decreasing frequency. Any aliased contribution from other bands will have their own different scintillation-induced imprint, and hence, is not expected to contribute to any significant net correlation. This forms the basis of our expectation for potential immunity of our scintillation correlation method against aliasing-induced contribution which disguises as off-pulse emission, and we assess it by using simulated dynamic spectrum over a spectral range several (7) times the nominal bandwidth of observation.

A detailed description of our simulation of diffractive scintillation is presented in Appendix B, and resultant dynamic spectrum spans 115.5 MHz (7x16.5 MHz) centered at 270 MHz, and covers a duration of about $1000t_s$ seconds. The time and spectral sampling here is $\sim t_s/4$ seconds and 64.45 kHz ($\sim \nu_d/20$), respectively.

This simulated dynamic spectrum, is treated as directly corresponding to an *on-pulse* intensity pattern. A small section ($\sim 180t_s$; or 3 hr, if $t_s = 60s$) of this pattern is shown in Figure 1, sampled across 1792 spectral channels and 700 time bins (out of the simulated duration spanning 4000 time bins).

The central spectral region, of 16.5 MHz width, is treated as the *observing* band, and the associated scintillation pattern is assumed to directly simulate an *observed on-pulse dynamic spectrum*. As an example, Figure 2 presents a zoomed portion over a short duration ($\sim 25t_s$, or say, 25 minutes), where the scintle scales in both the dimensions are clearly discernible.

Dynamic spectrum corresponding to the *off-pulse* region, on the other hand, is *constructed* by appropriately superposing the intensity variation simulated across the seven bands, following different assumed levels of genuine unpulsed (off-pulse) emission, and those of aliasing from contaminating bands, if any. For completeness, enabling a range of assessments, we consider the following three kinds of off-pulse dynamic spectra, as having (a) only genuine unpulsed emission, (b) genuine unpulsed emission plus contamination from aliasing, and (c) no genuine unpulsed component, but with only aliased contributions.

In (a) and (b), the dynamic spectral contribution as due to a genuine unpulsed emission is readily obtained from the on-pulse dynamic spectrum, suitably scaled by an assumed factor η . Unless mentioned otherwise, η is assumed to be 0.01. We assume, for simplicity, that the aliased bands, contributing in (b) and (c), are attenuated by also the same factor (i.e. 0.01 or -20 dB). The off-pulse dynamic spectra, across the same span (16.5 MHz, with 256 channels), wherein any aliased contribution from other bands is added together, with or without band-flips, as appropriate. An off-pulse dynamic spectrum thus simulated for the case (c), only with aliased contribution from only two bands adjacent to the observed band (i.e. immediate upper and lower band) on either side, is shown in Figure 3 (depicting a similarly zoomed section as in Figure 2).

The Figure 4 presents the auto-correlations, and the cross-correlation maps computed using the the respective dynamic spectra shown in Figure 2 and Figure 3.

The results in Table 1 are for the following two distinct cases of simulated off-pulse dynamic spec-

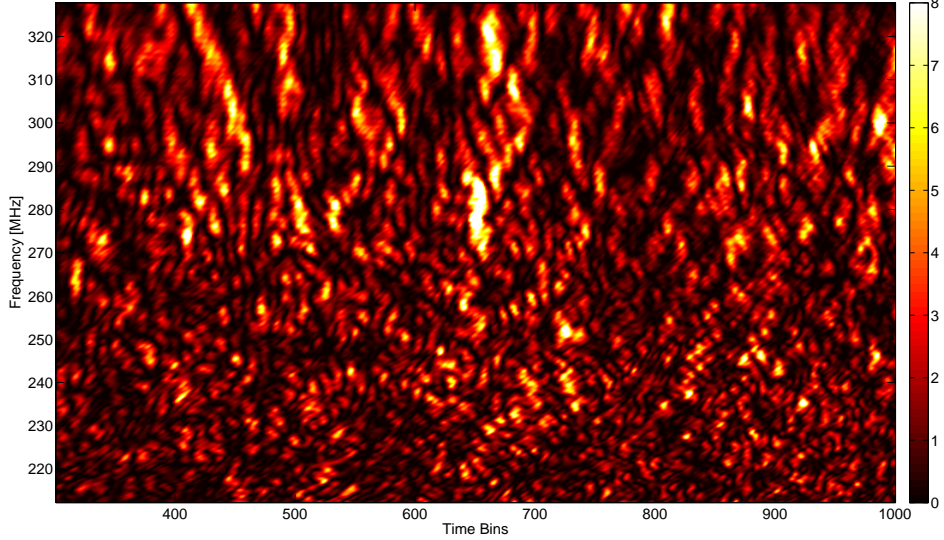


FIG. 1.— The simulated dynamic spectrum across a wide spectral span (bandwidth 7×16.5 MHz) around a central frequency of 270 MHz, but C_N^2 , D and S_d chosen such that this dynamic spectra have ν_d and t_d similar to that corresponding to central frequency 810 MHz for PSR B0329+54. The portion shown here is about one fourth of the simulated time span.

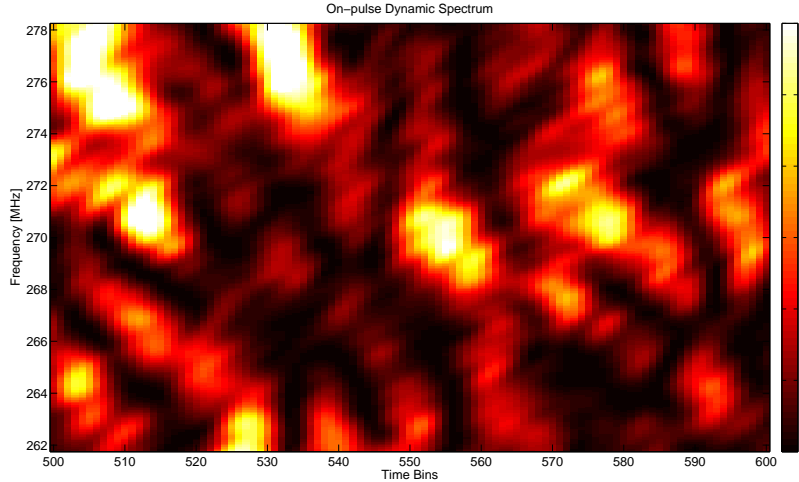


FIG. 2.— The simulated on-pulse dynamic spectrum across the observing band, obtained from scintillation pattern shown Figure 1.

trum; namely, for $\eta_{\text{true}} = 0.01$ and 0. In each case, the aliasing-induced contamination from adjacent spectral bands is explicitly included (with chosen attenuation), for aliasing-order (AO) ranging for 1 to 3, making a total of six versions of simulated off-pulse spectra. These are separately

used along with a common on-pulse dynamic spectrum to estimate η in each case. For example, an aliasing-order “k” corresponds to a spectral span of $k \cdot \Delta\nu_{\text{BW}}$ on either side of the observing band as being the source of contamination.

The estimates of uncertainty in η depend of the

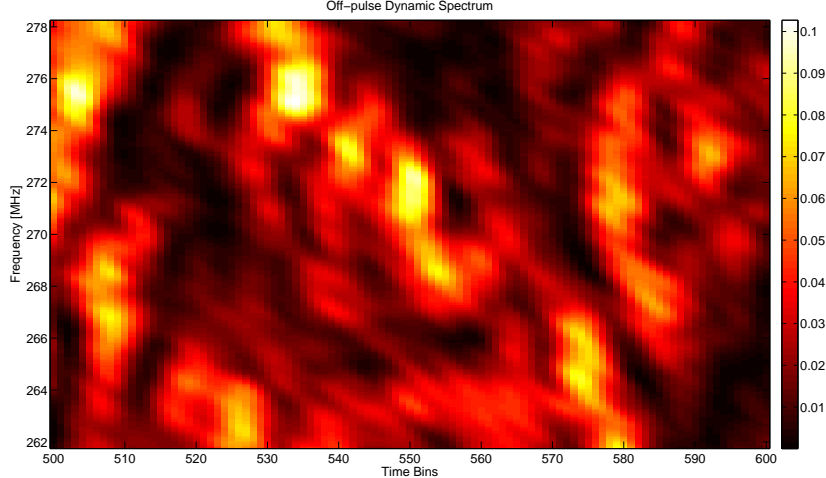


FIG. 3.— The simulated *off-pulse* dynamic spectra, corresponding to the *observing band* as in Figure 2, but obtained by including only the aliased contribution from the two adjacent bands around the observing band (taken from the simulated wide-band dynamic spectrum for the main pulse as shown in Figure 1). This corresponds the case (ii), i.e. no genuine off-pulse/unpulsed emission component, but contains only the contributions due to aliasing, disguising as apparent variations in the unpulsed intensity in the off-pulse region.

N_{eff} , which is computed following the same procedure as described in Section 2. In each case, having dynamic spectra that are same for the on-pulse, but differently constructed for the off-pulse region, the N_{eff} is computed based on the decorrelation scales seen in the latter (i.e. off-pulse) spectra. The decorrelation scales as seen to effectively broaden with the number of independent spectral patterns contributing to the constructed off-pulse dynamic spectra, as would be expected. The simulated intensities in the dynamic spectra are essentially exponentially distributed. These distributions would approach to Gaussian, when additive measurement uncertainties are significant. The overall positive bias in the estimates of η computed from the entire span is understood as due to the slow modulation of pulse intensity (owing to refractive scintillations) which is shared by the contaminants of the off-pulse dynamic spectrum. When the suggestion made in an earlier section is followed, i.e. η is estimated separately for each of the shorter spans, and such estimates combined appropriately, the average η estimate is largely free of such bias, without loss of sensitivity. This can be appreciated from the comparison of the results presented in Table 1.⁷

⁷ The 6 models correspond to 2 sets, with and without genuine unpulsed emission component, in each of the three aliasing-orders. Two estimates of η are presented for each

TABLE 1
THE ESTIMATED η , FOR THE 6 MODELS (2 CASES EACH).

AO	N_{eff}	$\eta \pm \sigma_{\eta}$ ($\eta_{\text{true}} = 0.01$)	N_{eff}	$\eta \pm \sigma_{\eta}$ ($\eta_{\text{true}} = 0$)
1 A	628	0.0099 ± 0.0007	736	0.0014 ± 0.0005
1 B		0.0111 ± 0.0006		0.0011 ± 0.0005
2 A	609	0.0139 ± 0.0009	609	0.0043 ± 0.0008
2 B		0.0106 ± 0.0008		0.0007 ± 0.0007
3 A	517	0.0137 ± 0.0012	511	0.0049 ± 0.001
3 B		0.0104 ± 0.001		0.0009 ± 0.0009

The η estimates in all considered cases are consistent with their respective model/assumed values η_{true} within the mentioned uncertainty. The N_{eff} changes systematically with aliasing-order, indicating possible increase in the decorrelation scales (ν_d and t_s).

The correlation maps in Figure 5 are presented to illustrate the implication of the relative location of the region corresponding to the intrinsic unpulsed/off-pulse emission, for a location offset of $0.1R_{LC}$. These are a result of our extended

model; A: using the entire span together, and B: using eight sub-spans separately for η estimation, and the weighted average of such estimates computed. The latter is largely free of the bias corrupting the former estimates. See the main text for details.

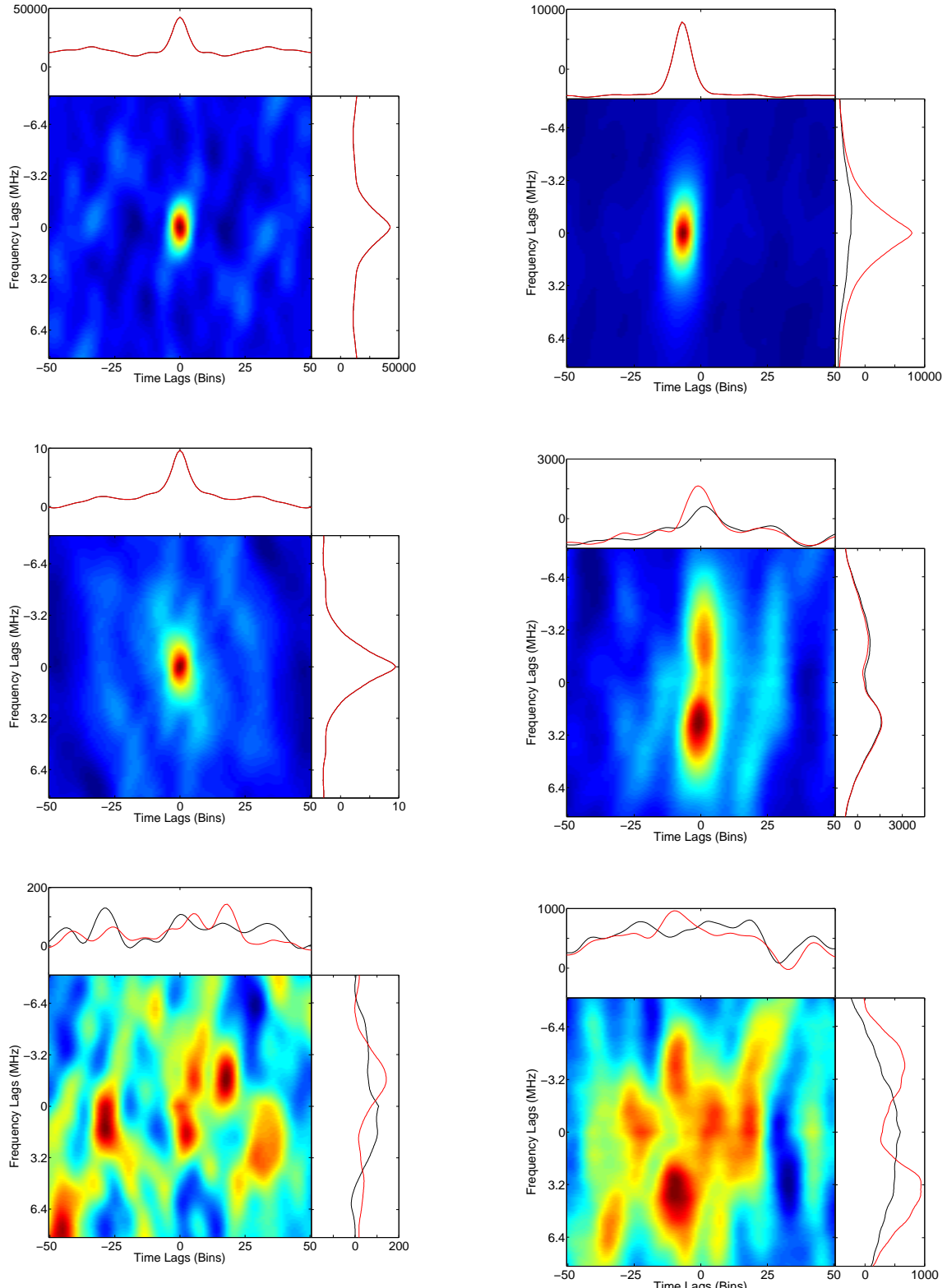


FIG. 4.— *Top*: Auto-correlation map of simulated on-pulse dynamic spectra of Figure 2. *Middle*: Auto-correlation map of simulated off-pulse dynamic of Figure 3. *Bottom*: Cross-correlation map of on-pulse and off-pulse dynamic spectra. In all these three sub-figures, the top plots are 1-D cut at zero time lag (black) and 1-D cut passing through maximum of the 2-D correlations(red) and side plots are that corresponding to frequency lags. The frequency-lag and the time-lag are in units of 64.45 kHz and $\sim t_5/5$ seconds, respectively. In 2-D color-maps, color *dark red* corresponds to highest magnitude and *dark blue* to lowest magnitude.

FIG. 5.— Cross-correlations of simulated on-pulse dynamic spectra and various off-pulse dynamic spectra. The off-pulse dynamic spectra are made from assuming their source separated from that of on-pulse by $0.1R_{LC}$ in, *top*: x-direction (our assumed direction of pulsars motion), *middle*: y-direction and *bottom*: at 45° to x-direction. All other notions in these figures are same as those mentioned in the caption of Figure 4.

simulations, to directly obtain special versions of off-pulse dynamic spectra (see the text at the end of Appendix B), and enable us to examine modification of cross-correlation signature for different magnitudes and specific orientations (\parallel , \perp and 45° to V) of location offsets (for unpulsed emission source) within the light cylinder. The corresponding correlation maps (such as in Figure 5), for different magnitude and orientation of the location offset, indeed show the expected qualitative correspondence (in terms of shift and/or reduction of the correlation peak, as discussed in Section 2.1) in all of the specific cases we simulated.

The above tests with simulated data demonstrate the sensitivity of our technique in reliably searching/estimating possible intrinsic unpulsed emission using pulsar dynamic spectra, and confirm its desirable immunity to possible contaminants of off-pulse dynamic spectra.

4. ILLUSTRATION OF OUR TECHNIQUE: A CASE STUDY WITH DATA ON B0329+54

We now apply our technique to data from observation on pulsar B0329+54, made using multi-band receiver system (MBR; Mann et al. 2013) with the Robert C. Byrd Green Bank Telescope (GBT), on July 25, 2009.

From among many pulsars observed in ten well separated bands simultaneously, we have chosen B0329+54 based on sensitivity considerations, given that it is one of the brightest pulsars known. Width of each band $\Delta\nu_{\text{BW}}$ is 16.5 MHz, and timespan of the observation Δt_{obs} is 1 hour. Other considerations include choice of the frequency band, as well as the resolutions in time and frequency, with which we can expect to see scintillation features in the the on-pulse dynamic spectrum. These choices depend largely on the decorrelation bandwidth and timescale, which are given by $\nu_d(\text{kHz}) = 59C_{-4}^{-1.2}\lambda^{-4.4}D^{-2.2}$ and $t_s(s) = 149C_{-4}^{-0.6}\lambda^{-1.2}D^{-0.6}v_7^{-1}$, respectively (Romani et al 1985⁸). Adequately fine sampling of the scintles, and ensuring as large a number of scintles as possible within the spectro-temporal span, require that $\delta\nu_{\text{res}} \ll \nu_d \ll \Delta\nu_{\text{BW}}$ and $\delta t_{\text{res}} \ll t_s \ll \Delta t_{\text{obs}}$. Based on these criteria, the data at 730 MHz and 810 MHz are found suitable, while other data at lower and higher frequencies did not meet these criteria. For B0329+54, at 730 MHz, the esti-

⁸ Romani et al. (1986) has some typographical errors in these expressions; a wrong exponent of C_{-4} in the expression for ν_d , and v instead of v_7 the expression for $t_s(s)$.

TABLE 2
RESULTS FROM THE DYNAMIC SPECTRAL
CROSS-CORRELATION ANALYSIS OF
SCINTILLATION DATA FOR THE ON- AND
OFF-PULSE REGIONS. THE ESTIMATES OF N_t
AND N_ν ASSUME A CONSERVATIVE VALUE OF
THE FILLING FACTOR $\kappa = 0.2$.

ν	730 MHz	810 MHz
N_t	~ 5	~ 4
N_ν	~ 3	~ 3
N_{eff}	14.4	12.7
σ_η	0.0017	0.0021
$\eta \pm \sigma_\eta$	0.0002 ± 0.0017	0.0013 ± 0.0021
η_{max}	0.0045	0.0066

mated ν_d and t_s are ~ 100 kHz to ~ 1800 kHz and 970 s to 240 s, respectively, at 810 MHz, the corresponding ν_d and t_s are ~ 200 kHz to ~ 2900 kHz and 1100 s to 270 s, respectively, for $C_N^2 \sim 3 \times 10^{-5}$ and $\sim 3 \times 10^{-4} m^{-20/3}$. Available measurements by Stinebring et al. (1996) and Wang et al. (2008) at 610 and 1540 MHz, respectively, imply ν_d and t_s to be about 750 kHz and 450 s, respectively, at our lower frequency. For comparison, our estimated decorrelation scales (from correlation analysis such as shown in Figure 8) of about 1 MHz, 360 s and 1.3 MHz, 400 s, at 730 and 810 MHz, respectively, are largely consistent with the above mentioned values, within the uncertainties. Our dynamic spectra have frequency resolution of 64.45 kHz, and time-resolution of 18 s, with 200 time bins across 3600 s.

The recorded raw voltage time sequences corresponding to a bandwidth of 16.5 MHz were analyzed to obtain dynamic spectra with frequency resolution of 64.45 kHz (i.e., across 256 channels). After suitable corrections for dispersion and gain compression,⁹ if any, dynamic spectra for various choices of ranges in the longitude were obtained separately. Figures 6 and 7 show these pairs of dynamic spectra, in which the spectral or time ranges affected by radio frequency inter-

⁹ When signal levels are even slightly larger than the limit within which a radio receiver has linear response, output power becomes less than that expected from its linear response, amounting to reduction in the gain. “Gain compression” refers to this reduction in gain, or non-linear response. In the context of dispersed pulsar signals, if not corrected, such a situation can cause a dip proportional to the pulse intensity, with a spread in longitude corresponding to the dispersion delay across the observed bandwidth. This effect can contaminate off-pulse region significantly, in cases of bright and high dispersion measure pulsars.

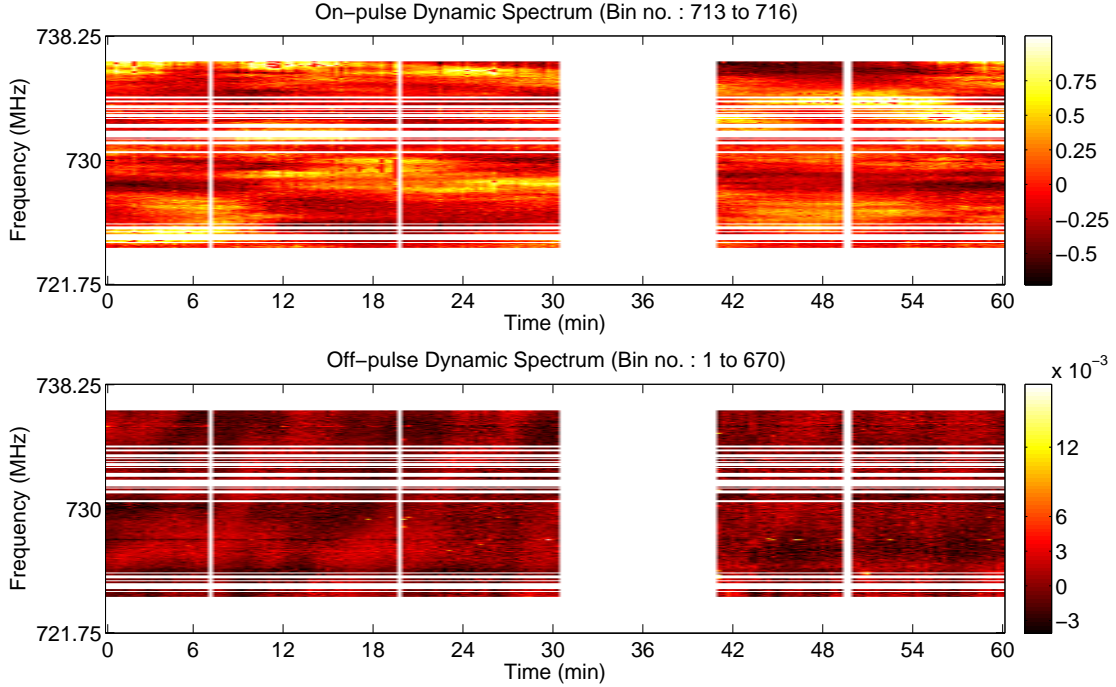


FIG. 6.— The observed on- and off-pulse dynamic spectra for B0329+54 at central frequency 730 MHz and bandwidth 16.5 MHz. The horizontal and vertical white stripes, corresponding to RFI channels and bad time-sections, are excluded from analysis.

ference have been removed.

For our data, after removing bad time-sections and RFI channels, we have performed the dynamic spectral correlations, to estimate various quantities mentioned above, including the measure of correlation η . More specifically, we estimate N_t , N_ν , N_{eff} , η and σ_η , along with η_{max} , as listed in Table 2.

As is apparent from these estimates, the off-pulse emission can be said to be less than about 0.5% of the main pulse flux density (corresponding a 3- σ limit). The present reduction in the uncertainties in η is moderate, in comparison with the hard limit η_{max} , and is consistent with the relatively small statistics (i.e. N_{eff}).

At this stage, our presentation of these results is mainly as an illustration, but with improved spectro-temporal span of the data (i.e. large N_{eff}), we can expect a significant refinement in these estimations and their uncertainties.

As can be seen readily from the 1-d plots corresponding to the auto-correlations shown in Figure

8, the random measurement noise de-correlates at non-zero lags, and the sharp drop in the auto-correlation with respect to its value at zero-lag provides a ready estimate of its relative contribution (i.e. σ_{on}^2 or σ_{off}^2), which is to be discounted while estimating decorrelation bandwidth or time-scale.

From the cross-correlation map (the bottom plot in Figure 8), and in general, the level of cross-correlation, or the lack of it, can be assessed across the respective lags, and interpreted either in terms of upper limits on the unpulsed emission intensity, or possible separation of the associated emission region from that of the main-pulse emission.

5. DISCUSSION AND CONCLUSIONS

The new technique proposed here, for searching for intrinsic off-pulse/unpulsed radiation for pulsars, is inspired by the expectation that such emission originating from apparent location(s) matching to or in the *vicinity* of that of the pulsed component (compared at their respective retarded emission times) would also carry a scintillation imprint similar to that measurable for the pulse in-

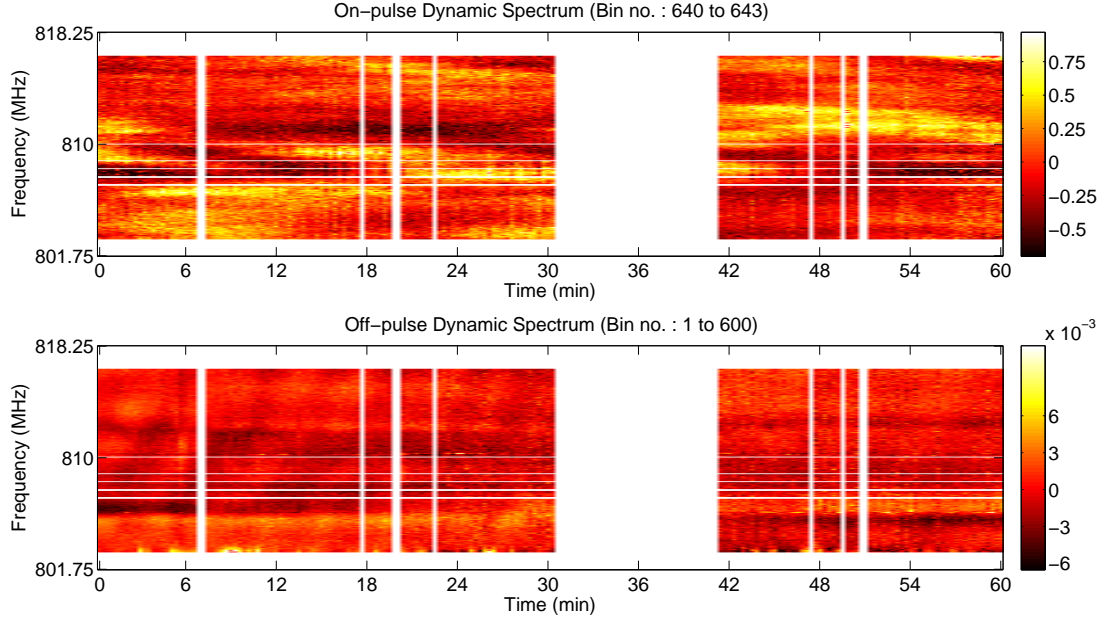


FIG. 7.— Similar dynamic spectra as in Figure 1, but now for the band around 810 MHz.

tensity.

Needless to say that a systematic search for unpulsed emission at a range of frequencies, with appropriate spectro-temporal resolution and spans, will naturally be rewarding. On the other hand, for data sets at sufficiently nearby frequencies, a combined estimate (or upper limit) for η can be obtained. For example, such an upper limit (3σ) for unpulsed intensity of B0329+54 would be 0.4%, based on the data at the two frequencies.

Since our method, although a truly high angular resolution probe, is based on longitude-resolved dynamic spectral information, it can be expected to be applied to most of the archived observations on pulsars, made from single-dish and synthesis telescopes, in addition to future observations, as long as the scintles, or the refractive fringing when present, are at least Nyquist sampled. In fact, it would not be surprising to see a massive initiative to search of the continuous/unpulsed emission in the near future, using existing data and new observations.

Although the relevant correlation would reduce exponentially with increasing apparent angular offset $\Delta S/z$ (Cordes et al. 1983) of the source to be searched, opportunity to detect significant peak in the correlation map (at a non-zero lag in

time) is to be expected when the orientation of the offset is along the pattern velocity (or within an alignment margin of $(S_d/\Delta S)^c$), as illustrated in our simulations. Interestingly, given the reported pulsar spin-velocity alignment, for young pulsars in particular (Johnston et al. 2005), the location offset along latitudinal direction is likely to be along the pattern velocity, when the scintillation speed is dominated by pulsar motion. Regardless of the possible apparent location of the region responsible for unpulsed emission, if any, within the light-cylinder, it is unlikely that the associated key morphology (say, w.r.t. rotation axis) would differ significantly from pulsar to pulsar. This combined with the expected variety in the orientation of the *apparent* velocity of the diffractive scintillation pattern (again viewed with respect to the pulsar spin-axis) and in S_d (depending on sight-line and frequency), suggests that there would be adequate number of known pulsars offering conducive situation for the proposed probe to be rewarding, in either detecting their elusive continuous emission, or ruling it out to the extent possible.

In summary, the existence of unpulsed emission from pulsars is yet to be fully established, let alone be understood. However, if detected unambiguously, any unpulsed radio radiation intrin-

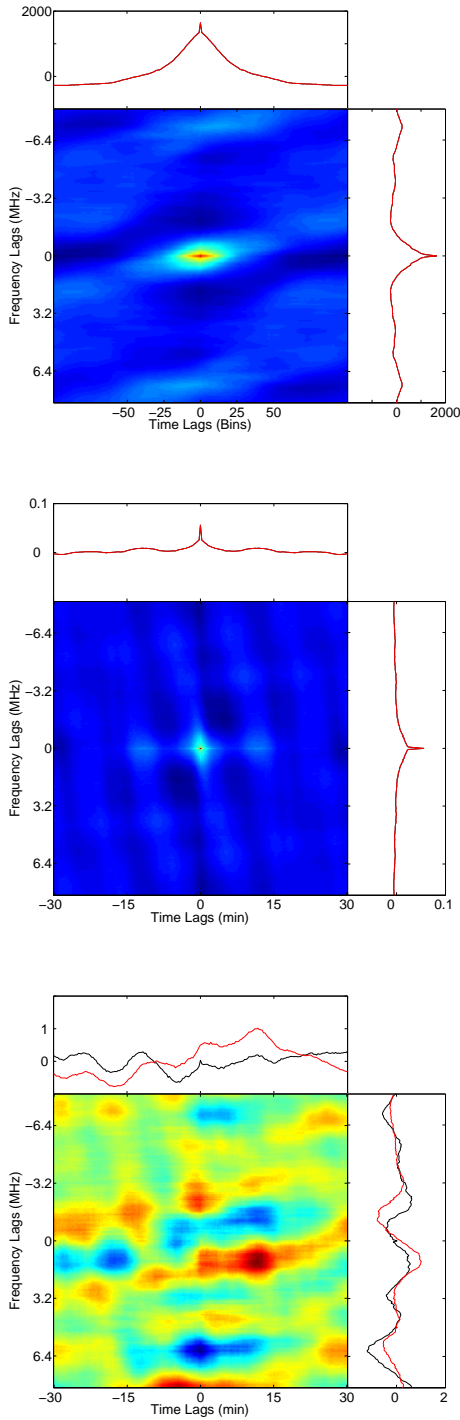


FIG. 8.— The correlation maps corresponding dynamic spectra of Figure 6. *Top*: Auto-correlation of on-pulse dynamic spectra. *Middle*: Auto-correlation of off-pulse dynamic spectra. *Bottom*: Cross-correlation of on-pulse and off-pulse dynamic spectra. Other details of the figure are same as mentioned in Figure 4.

sic to pulsars would indeed be a precious token of the mysteries of emission mechanism in radio pulsars that are yet to be unraveled, and could provide important missing clue to further our understanding of the key processes at work. Our proposed detection method, exploiting the resolving power of the interstellar telescope, as a powerful tool for reliable and sensitive search/detection of unpulsed/off-pulse emission, should open a new window for this promising exploration.

We gratefully acknowledge contribution from Karishma Bansal in the very early phase of this work (during her Visiting Studentship at the Raman Research Institute). We thank our anonymous referee for constructive comments and suggestions.

REFERENCES

Armstrong, J. W., Cordes, J. M., & Rickett, B. J. 1981, *Nature*, 291, 561

Armstrong, J. W., Rickett, B. J., & Spangler, S. R. 1995, *ApJ*, 443, 209

Bartel, N., Cappallo, R. J., Ratner, M. I., Rogers, A. E. E., Shapiro, I. I., & Whitney, A. R. 1984. VLBI and Compact Radio Sources, p. 275, eds Fanti, R., Kellermann, K. & Setti, G., Reidel, Dordrecht, Holland.

Basu, R., Athreya, R., & Mitra, D. 2011, *ApJ*, 728, 157

Basu, R., Mitra, D., & Athreya, R. 2012, *ApJ*, 758, 91

Blandford, R. D., Ostriker, J. P., Pacini, F., & Rees, M. J. 1973, *A&A*, 23, 14

Born, M., & Wolf, E. 1980 Principles of optics: electromagnetic theory of propagation, interference and diffraction of light. (808 pages.) New York: Pergamon Press.

Coles, W. A., Filice, J. P., Frehlich, R. G., & Yadlowsky, M. 1995, *Appl. Opt.*, 34, 2089

Cordes, J. M., Boriakoff, V., & Weisberg, J. M. 1983, *Astrophys. J.*, 268, 370

Cordes, J. M., & Lazio T. J. 1991, *ApJ*, 376, 123

Cordes J. M., Pidwerbetsky A., & Lovelace R. V. E. 1986, *ApJ*, 310, 737

Cordes, J. M., & Wolszczan, A. 1988, In Radio wave scattering in the interstellar medium, AIP Conf. Proc., 212, 17

Frail, D. A., Kulkarni, S. R., Nicastro, L., Feroci, M., & Taylor, G. B. 1997, *Nature*, 389, 261

Goodman, J., & Narayan, R. 1985, *MNRAS*, 214, 519

Gupta, Y., Bhat, N. D. R., & Rao, A. P. 1999, *ApJ*, 520, 173

Gupta, Y., Rickett, B. J., & Lyne, A. G. 1994, *MNRAS*, 269, 1035

Hankins, T. H., Moffett, D. A., Novikov, A., & Popov, M. 1993, *ApJ*, 417, 735

Hewish, A., Bell, S. J., Pilkington, J. D. H., Scott, P. F., & Collins, R. A. 1968, *Nature*, 217, 709

Huguenin, G. R., et al. 1971, *Nature Phys. Sci.*, 234, 50

Johansson, E. M., & Gavel, D. T. 1994, *Proc. SPIE* 2200, 372

Johnston, S., et al. 2005, *MNRAS*, 364, 1397

Lovelace, R. V. E. 1970, Ph.D. Thesis, Cornell University

Lovelace, R. V. E., Salpeter, E. E., Sharp, L. E., & Harris, D. E. 1970, *ApJ*, 159, 1047

Maan, Y., et al. 2013, *ApJS*, 204, 12

Macquart, J.-P., & de Bruyn, A. G. 2006, *A&A*, 446, 185

Narayan, R. 1988, In Radio wave scattering in the interstellar medium, AIP Conf. Proc., 174, 17

Pen, U.-L., Macquart, J.-P., Deller, A. T., & Brisken, W. 2014, *MNRAS*, 440, L36

Perry, T. E., & Lyne, A. G. 1985, *MNRAS*, 212, 489

Rathnasree, N., & Rankin, J. M. 1995, *ApJ*, 452, 814

Rickett, B. J. 1988, in Radio Wave Scattering in the Interstellar Medium, AIP Conf. Proc., 174, 2

Romani, R. W., Narayan, R., & Blandford, R. 1986, *MNRAS*, 220, 19

Stinebring, D. R., Faison, M. D., & McKinnon, M. M. 1996, *ApJ*, 460, 460

Strom, R. G., & Van Someren Greve, H. W. 1990, *Ap&SS*, 171, 351

Wang, N., Yan, Z., Manchester, R. N., & Wang, H. X. 2008, *MNRAS*, 385, 1393

Wolszczan, A., & Cordes, J. M. 1987, *ApJ*, 320, L35

APPENDIX

A: ALIASING IN DYNAMIC SPECTRA, AND POSSIBLE CONTAMINATION IN THE OFF-PULSE REGION

In this section, we discuss and illustrate how the observed data, and the off-pulse region in particular, be affected if the spectral filtering in the receiver chain were to be imperfect, allowing a non-zero fraction of sky signal out side the band of interest to pass through, even though attenuated significantly. Although, in practice, a variety of non-idealities in spectral filtering are possible¹⁰, for illustration purpose, we consider a simple case of the band-defining filter having a non-zero response in adjacent spectral ranges on either side of the intended band of observation.

It is easy to see that the contribution from a dispersed pulse in these out-of-band spectral regions would be aliased in the Nyquist sampled band of interest. On dedispersion, these aliased contributions from the *folded* bands would not only spill out side the pulse window, but can systematically spread across a large part of the off-pulse longitudes, and could disguise as off-pulse emission. For an illustrative example of this effect, lets assume that the filter function over the desired band (of width = BW) is flat, as corresponding to a perfect rectangular filter, but this non-ideal filter offers finite, though high, attenuation in other spectral regions. In our simulation, we consider the out-of-band region on either side to be 3 times wider than BW , and relative attenuation to be 20 dB, such that the filter response $F(\nu)$

¹⁰ The key filtering stages include, a) image-band rejection before heterodyne or mixing stage, and b) band-defining before digitization (at Nyquist rate) of signal either at baseband or that located around a chosen center frequency (where harmonic or band-pass sampling at Nyquist rate is employed).

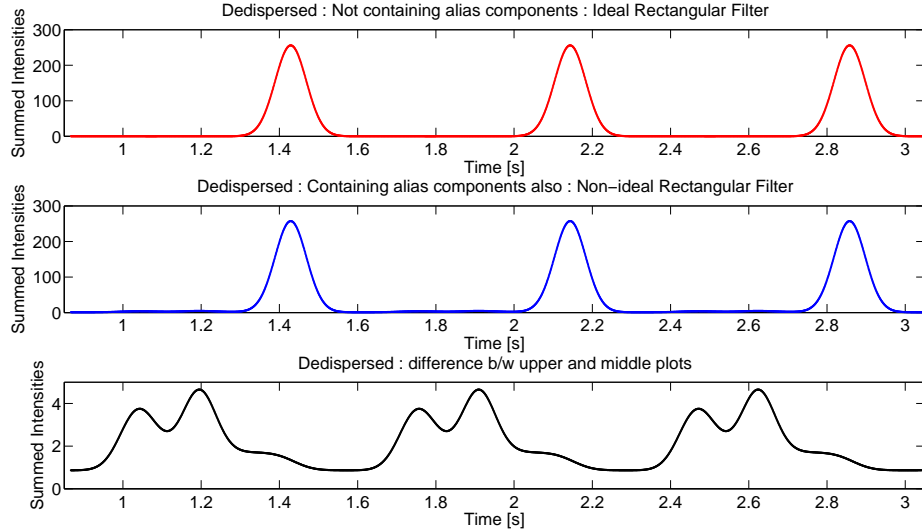


FIG. A1.— A simulated dedispersed pulse sequence in the case of an ideal filter function is shown in the top panel, for reference. A similarly simulated and dedispersed time sequence resulting from aliasing from adjacent bands is presented in the middle panel. The difference between these two sequences (as shown in the bottom panel) provides an illustration of the contamination due to aliasing effects. For details, please refer to the text in this appendix.

$$F(\nu) = \begin{cases} 1, & |\nu - \nu_c| \leq 0.5BW, \\ 0.01, & 0.5BW \leq |\nu - \nu_c| \leq 3.5BW, \\ 0, & \text{otherwise} \end{cases} \quad (\text{A1})$$

where, ν_c is the center frequency of observation.

Assuming a train of Gaussian pulses from a pulsar, the intensity pattern across time and frequency can be expressed as

$$I(\nu, t) = I_0 \exp\{-(t - \tau(\nu))^2 / (2\sigma^2)\} \quad (\text{A2})$$

where, P is the pulsar period, σ is the standard width of the Gaussian, n is number of periods defining the time span of the simulated sequence. The dispersion delay at frequency ν , with respect to that at a reference frequency ν_{ref} , is given by

$$\tau(\nu) = 4.15 \times 10^3 DM \left[\frac{1}{\nu^2} - \frac{1}{\nu_{\text{ref}}^2} \right] \quad (\text{s}) \quad (\text{A3})$$

where DM is the dispersion measure in pc cm^{-3} and the frequencies are in MHz. A dynamic spectrum containing dispersed pulses was simulated assuming $BW = 16$ MHz centered at $\nu_c = 300$ MHz, $\sigma = 0.04$ s, and for pulsar parameters similar to that of B0329+54 ($DM = 26.77 \text{ pc cm}^{-3}$, $P = 0.714472578$ s).

The top panel of Figure A1 (or 8) shows the dedispersed pulse sequence when no aliasing of sky signal occurs from outside of the desired band of bandwidth BW (a case of ideal filtering). The middle panel shows a similarly obtained sequence, but now including aliasing (of remaining small level of sky signal) from the adjacent bands as described above. Note that the dispersed pulse contribution from the aliased adjacent bands would be at a much lower level, but will make its appearance in the off-pulse region. These contributions will occupy different longitude spreads after dedispersion, depending on the alias order, in addition to the DM and P . Significant contamination in both the on-pulse and the off-pulse regions, as result of aliasing, is apparent from the difference between the sequences in the top two panels, as shown in the bottom panel. Here, we have deliberately used a lower ν_c ($=300$ MHz), than those for the data we present (i.e. 730 MHz or 810 MHz), so that the mentioned contamination is more pronounced.

B: SIMULATION OF DIFFRACTIVE INTERSTELLAR SCINTILLATION (DISS) AND DYNAMIC SPECTRA

The two main steps in simulation of DISS dynamic spectra, using a thin-screen approximation, are: (i) generation of a random phase screen following an assumed spatial distribution of electron density irregularities in the intervening ISM, which modifies the emerging wave-front, and (ii) calculation of resultant intensity, of the received signal at the observer's location, as a function frequency and time.

As mentioned already, the most accepted 3D spatial power spectral description of the turbulent ISM is a power-law spectrum across spatial frequency q , ranging from q_{\min} to q_{\max} , (Armstrong et al. 1995)

$$P_{3N}(q_x, q_y, q_z) = C_N^2 q^{-\beta}; \quad q = \sqrt{q_x^2 + q_y^2 + q_z^2} \quad (B1)$$

where, C_N^2 is the level of turbulence, and the power-law index $\beta = 11/3$ for the Kolmogorov turbulence. Armstrong et al. (1995) have given evidence of the validity of Equation B1 for $q_{\min} = 10^{-12} \text{ m}^{-1} < q < q_{\max} = 10^{-6} \text{ m}^{-1}$, and have derived the typical turbulence strength $C_N^2 \sim 10^{-3} \text{ m}^{-20/3}$, but the C_N^2 can deviate significantly from this typical value, depending on direction and distance to the source.

A convenient way to study propagation effects due to this 3-D distribution of refractive index irregularities in the ISM is to model the modification of the incident wave-front by an equivalent thin phase-changing screen, located between the source and the observer. We use this thin screen approximation (see Lovelace 1970; Romani et al. 1986) for our present simulations, wherein the equivalent 2-D spatial power spectrum ($P_{2\phi}$) of the phase deviation ϕ is given by

$$\begin{aligned} P_{2\phi}(q_x, q_y) &= 2\pi z(\lambda r_e)^2 P_{3N}(q_x, q_y, q_z = 0) \\ &= 2\pi z(\lambda r_e)^2 C_N^2 \left(\sqrt{q_x^2 + q_y^2} \right)^{-\beta} \end{aligned} \quad (B2)$$

where, z is the distance to the source, $r_e = 2.82 \times 10^{-15} \text{ m}$ is the classical radius of the electron, and λ is the wavelength of the propagating radiation.

Generation of Equivalent Thin Phase-Screen using FFT-Based Technique

The spatial power spectrum of the equivalent 2-D thin screen and the associated distribution of the random phase deviation $\phi(x, y)$ across that screen in transverse plane (x, y) have the following Fourier relationship

$$\phi(x, y) = \int_{-\infty}^{+\infty} \int_{-\infty}^{+\infty} g(q_x, q_y) \sqrt{P_{2\phi}(q_x, q_y)} \exp[-j2\pi(xq_x + yq_y)] dq_x dq_y \quad (B3)$$

i.e., $\phi(x, y)$ is the (inverse) Fourier transform of the product $g(q_x, q_y) \sqrt{P_{2\phi}(q_x, q_y)}$, where $g(q_x, q_y)$ is a Hermitian-symmetric complex Gaussian variable representing zero-mean white noise process, with unity variance (Johansson & Gavel 1994). We obtain $\phi(x, y)$ distribution using the above relation, employing FFT technique for computational ease.

The discrete form needed for simulation, of the Equation B3, for a square screen, ϕ , made-up of $N \times N$ grid points, is

$$\phi = 2\pi(2\pi)^{-\beta/2} (N\Delta r)^{-1+\beta/2} \sqrt{2\pi z(\lambda r_e)^2 C_N^2} [\mathcal{FT}^{-1}\{g M_0\}] \quad (B4)$$

where, Δr is spatial sampling interval, g is a $N \times N$ matrix (the procedure to obtain it is explained in the following) and M_0 is also a $N \times N$ matrix whose elements are $M_0(i, j) = [(i - N_c)^2 + (j - N_c)^2]^{-\beta/4}$, where the origin is defined at $N_c = N/2 + 1$, and the contribution at zero spatial frequency is set to zero, i.e. $M(N_c, N_c) = 0$. The recipe for getting the Gaussian random matrix g is as follows:

- (i) generate a complex matrix (say) M of size $N \times N$, whose elements are $a + jb$, where, $j = \sqrt{-1}$, a and b are independent Gaussian random numbers with zero mean and unity variance.
- (ii) obtain the 2-D discrete Fourier transform of ' M ', which will be the required matrix g ($g = \mathcal{FT}^{-1}\{M\}$).

Electric Field Distributions and Resultant Intensity in the Observer's Plane

Having generated $\phi(x, y)$ (i.e., the discrete ϕ , Equation B4), the electric field distribution at the thin screen can be given by

$$E_s(x, y) = \exp(-j\phi(x, y)). \quad (B5)$$

In the thin screen approximation, the ray optics is applicable and so the electric field received at any point (ξ, η) on the observer plane, can be represented by the Fresnel-Kirchhoff integral (Born & Wolf 1980)

$$E_O(\xi, \eta) = \frac{e^{-j\pi/2} e^{j2\pi z/\lambda}}{2\pi r_f^2} \int \int \exp \left[j\phi(x, y) + j \frac{(x - \xi)^2 + (y - \eta)^2}{2r_f^2} \right] dx dy \quad (B6)$$

where, $r_f = \sqrt{\lambda z / 2\pi}$. This integral can be either calculated from 2-D numerical integration or methods using Fourier transform. We have used angular spectrum method to calculate the electric field, i.e., via following relation (in discrete form)

$$E_O = \mathcal{IFT}\{\mathcal{FT}\{h(x, y)\} \mathcal{FT}\{\exp(-j\phi)\}\} \quad (B7)$$

where, $h(x, y)$ is called transfer function. By use of the above method to get E_O , the spatial sampling interval at the observer's plane will be the same Δr as that of phase distribution of the thin phase screen. So corresponding to each value of input frequency/wavelength, we will have phase distribution ϕ of the thin screen (in discrete form a matrix of size say $N \times N$) and the electric field E_O at the observer's plane (again a matrix of size $N \times N$). From this matrix E_O , we select a spatial 1D cut, say $E_O(r)$, which may be an arbitrarily chosen row or column, and obtain $E_O(\nu, r)$ by varying only ν in uniform steps over the range of interest. The spatio-spectral description of observed intensity is trivially obtained as $I_O(\nu, r) = |E_O(\nu, r)|^2$. This $I_O(\nu, r)$ can be translated into $I_O(\nu, t)$, i.e. the dynamic spectrum, by assuming a velocity V_{trans} along r for the intensity pattern in the observer's plane, which depends on the relative transverse velocities of the pulsar, the scattering medium and the observer.

Our Simulation Parameters and Results

Diffractive effects correspond to spatial frequency range $q \sim 10^{-8} \text{ m}^{-1}$ to 10^{-6} m^{-1} of the ISM irregularities (Stinebring 1996; Rickett 1988; Narayan 1988; Wang, Manchester 2008). We have used a square (scattering) screen so sampling interval, say Δr , in x and y directions are equal, i.e. $\Delta x = \Delta y = \Delta r$. The Nyquist sampling criteria demands $\Delta r = 1/(2q_{\text{max}})$. What size of the phase screen will be suffice for simulation of DISS? The observer receives radiation from a cone of half-angle $\theta_S \approx r_{\text{ref}}/z \approx r_{\text{mp}}/z \approx \lambda/(2\pi S_d)$, (Cordes 1986) where, r_{ref} is refractive length scale, r_{mp} is multi-path propagation length scale (strong scintillation), S_d is diffractive length scale, z is distance from the observer to the thin screen and λ is the wavelength of the radiation from pulsar. So to properly simulate DISS, the phase screen size r_{max} should be at least $\sim r_{\text{mp}} \approx r_f^2/S_d$ in each of the two dimensions. Hence the required number of grid points N across r_{mp} , for a $N \times N$ matrix describing the screen, would be $N \geq r_{\text{max}}/\Delta r = 2q_{\text{max}}r_f^2/S_d$. Thus for the case of our data on B0329+54, where $\nu=810 \text{ MHz}$ and $z = 1.44 \text{ kpc}$, $r_{\text{mp}} \sim 10^{11} \text{ m}$. To satisfy the criteria $\Delta r \leq 1/(2q_{\text{max}})$, the required $N \sim 2^{18}$ [$N = 10^{11}/(5 \times 10^5) \sim 2 \times 10^5 \sim 2^{18}$]! To generate a phase screen of this overwhelmingly large dimension, of order $2^{18} \times 2^{18}$, and the subsequent Fourier analysis involving bigger dimension (i.e., $2^{19} \times 2^{19}$) is not only computationally intensive (even with use of FFTs), but well beyond the readily available computing resources.

However, we note the *red* nature of the underlying spatial spectrum of phase variation $P_{2\phi} \propto q^{-\beta}$ (β is +ve). The associated structure function for phase ϕ , at a given scale r can be expressed as $D_\phi(r) = (1^c)^2 (r/S_d)^{(\beta-2)}$, given that for the diffractive (or the coherence) scale S_d , the phase structure function is 1 radian² (Armstrong et al. 1995). Since contribution to phase fluctuations from smaller spatial scales is expected to decrease rapidly, for the relevant values of β , we consider revision of the sampling scale Δr , such that $D_\phi(\Delta r) \leq \Delta\phi_{\text{min}}^2$, for the desired small phase variation $\Delta\phi_{\text{min}}$ that is to be sampled duly. With this criterion, and recalling Equation 8, we express the required grid dimension as

$$N \geq \frac{(\nu/\nu_d)}{(\Delta\phi_{\text{min}})^{2/(\beta-2)}} \quad (B8)$$

For example, with $\Delta\phi_{\min} = 0.1$ radian, and $\beta = 11/3$, $N \geq 16(\nu/\nu_d)$. Choosing a suitable ratio (ν/ν_d) , say 200, the requirement of $N \geq 3200$ appears feasible with computational constraints, i.e. without needing supercomputers, and more importantly, without compromising significantly on the details of the phase screen.

In our present simulations, we have used $\nu_d \sim 1.35$ MHz, to keep reasonable correspondence with the discussed observations, but use a relatively smaller ν of 270 MHz. We use $N = 4096$, so that the screen and the diffraction patterns are sampled with adequate details (corresponding to $\Delta r = 5 \times 10^5$ m and $r_{\max} \sim 2 \times 10^9$)¹¹, and the resultant dynamic spectrum suffices for demonstrating the key aspects of our technique. It is worth pointing out that now the Fresnel scale r_f and z are artificially small and C_N^2 is correspondingly large, as a result of the spatial dynamic range we have chosen. However, the scale of direct relevance to us, that is the diffraction pattern scale S_d corresponds to typical 4 samples across r , implying $(t_s/4)$ as the sampling interval in the dynamic spectrum. The overall time scale, and t_s , can be defined by choice of the velocity V_{trans} , if required. In any case, the simulated time span corresponds to $\sim 1000t_s$.

For completeness, to examine the sensitivity of the correlation technique to the relative location off-pulse emission region, we extended our simulations to obtain the off-pulse dynamic spectra separately from that for the pulsed component. Using the common description for the phase pattern, we added a suitable extra phase-gradient to it for simulating new phase screen, corresponding to the location offset, and used the resultant intensity pattern for constructing off-pulse dynamic spectra. The magnitude and direction of the location offset were varied, and the resultant cross-correlation maps were examined (see Figure 5).

¹¹ It is worth noting that now the Fresnel scale r_f and z are artificially small and C_N^2 is correspondingly large, as a result of the spatial dynamic range we have chosen.